UNCLASSIFIED

AD NUMBER
ADB005139
LIMITATION CHANGES
TO: **Approved for public release; distribution is unlimited.**
FROM: **Distribution authorized to U.S. Gov't. agencies only; Test and Evaluation; JUN 1975. Other requests shall be referred to Air Force Weapons Laboratory, DYS, Kirtland AFB, NM 87117.**
AUTHORITY
afwl ltr, 7 apr 1977

THIS PAGE IS UNCLASSIFIED

THIS REPORT HAS BEEN DELIMITED
AND CLEARED FOR PUBLIC RELEASE
UNDER DOD DIRECTIVE 5200.20 AND
NO RESTRICTIONS ARE IMPOSED UPON
ITS USE AND DISCLOSURE.

DISTRIBUTION STATEMENT A

APPROVED FOR PUBLIC RELEASE;
DISTRIBUTION UNLIMITED.

AFWL-TR-74-231

AFWL-TR-
74-231

AD B005139

LASER-PLASMA INTERACTIONS IN EXPLODING WIRES

Robert M. Wyatt, Lt, USAF

June 1975

Final Report for Period March 1973 - August 1974

Distribution limited to US Government agencies only because of test and evaluation of military systems (Jul 75). Other requests for this document must be referred to AFWL (DYS), Kirtland Air Force Base, New Mexico 87117.

DDC
RECEIVED
JUL 18 1975
B

AIR FORCE WEAPONS LABORATORY
Air Force Systems Command
Kirtland Air Force Base, NM 87117

This final report was prepared by the Air Force Weapons Laboratory, Kirtland Air Force Base, New Mexico under Job Order 88091701. Lt Robert M. Wyatt (DYS) was the Laboratory Project Officer-in-Charge.

When US Government drawings, specifications, or other data are used for any purpose other than a definitely related Government procurement operation, the Government thereby incurs no responsibility nor any obligation whatsoever, and the fact that the Government may have formulated, furnished, or in any way supplied the said drawings, specifications, or other data, is not to be regarded by implication or otherwise, as in any manner licensing the holder or any other person or corporation, or conveying any rights or permission to manufacture, use, or sell any patented invention that may in any way be related thereto.

This technical report has been reviewed and is approved for publication.

Robert M. Wyatt
ROBERT M. WYATT
Lieutenant, USAF
Project Officer

FOR THE COMMANDER

Thomas C. May
THOMAS C. MAY
Major, USAF
Chief, X-Ray Simulation Branch

David M. Ericson Jr
DAVID M. ERICSON, JR.
Lt Colonel, USAF
Chief, Technology Division

DO NOT RETURN THIS COPY. RETAIN OR DESTROY.

UNCLASSIFIED

SECURITY CLASSIFICATION OF THIS PAGE (When Data Entered)

REPORT DOCUMENTATION PAGE

READ INSTRUCTIONS BEFORE COMPLETING FORM

1. REPORT NUMBER
AFWL-TR-74-231

2. GOVT ACCESSION NO.

3. RECIPIENT'S CATALOG NUMBER

4. TITLE (and Subtitle)
LASER-PLASMA INTERACTIONS IN EXPLODING WIRES

5. TYPE OF REPORT & PERIOD COVERED
Final Report
March 1973 - August 1974

6. PERFORMING ORG. REPORT NUMBER

7. AUTHOR(s)
Robert M. Wyatt, Lt, USAF

8. CONTRACT OR GRANT NUMBER(s)

9. PERFORMING ORGANIZATION NAME AND ADDRESS
Air Force Weapons Laboratory
Kirtland Air Force Base, New Mexico 87117

10. PROGRAM ELEMENT, PROJECT, TASK AREA & WORK UNIT NUMBERS
Program Element 62601F
Project 8809, Task 1701

11. CONTROLLING OFFICE NAME AND ADDRESS
Air Force Weapons Laboratory
Kirtland Air Force Base, New Mexico 87117

12. REPORT DATE
July 1975

13. NUMBER OF PAGES
44

14. MONITORING AGENCY NAME & ADDRESS(if different from Controlling Office)
Air Force Weapons Laboratory
Kirtland Air Force Base, New Mexico 87117

15. SECURITY CLASS. (of this report)
UNCLASSIFIED

15a. DECLASSIFICATION/DOWNGRADING SCHEDULE

16. DISTRIBUTION STATEMENT (of this Report)
Distribution limited to US Government agencies only because of test and evaluation of military systems (Jul 75). Other requests for this document must be referred to AFWL (DYS), Kirtland Air Force Base, New Mexico 87117.

17. DISTRIBUTION STATEMENT (of the abstract entered in Block 20, if different from Report)
Same as block 16.

18. SUPPLEMENTARY NOTES

19. KEY WORDS (Continue on reverse side if necessary and identify by block number)
CO_2 Laser
Plasma
Exploding Wires
Corona Model
DULAH

20. ABSTRACT (Continue on reverse side if necessary and identify by block number)
The preformed plasma of an exploding wire is an interesting plasma for laser interaction studies--both for basic physics and for applications. Theoretical studies have been made of: (1) the initiation of exploding wires by a capacitor bank; (2) the optical properties of the laser interaction with this plasma; (3) the scaling of laser heating with laser pulse shape, pulse width (10 to 80 nanoseconds), power, and energy (40 to 40,000 joules) for the CO_2 laser and aluminum wire interaction. Results indicate that this interaction is definitely of sufficient interest to justify further study.

DD FORM 1 JAN 73 1473 EDITION OF 1 NOV 65 IS OBSOLETE

UNCLASSIFIED

SECURITY CLASSIFICATION OF THIS PAGE (When Data Entered)

CONTENTS

Section		Page
I	INTRODUCTION	3
II	CORONA MODEL CALCULATIONS OF AVERAGE IONIZATION LEVEL AND ENERGY	5
III	RAY TRACING STUDIES OF EXPLODING WIRES	12
IV	INITIATION AND LASER HEATING OF EXPLODING WIRE PLASMAS	24
	REFERENCES	41
	DISTRIBUTION	42

SECTION I

INTRODUCTION

Heating a preformed plasma with a laser has been of interest because of basic physics and a wide variety of applications. Some previous calculations have been directed toward the interaction of CO_2 lasers with the plasma created in the dense plasma focus (DPF) (ref. 1). These calculations showed that the presence of small amounts of high-Z impurities greatly reduce the electron temperature achievable in heating the DPF, as well as affecting the intensity of the line, recombination, and bremsstrahlung radiation produced by the plasma. Thus, to treat situations in which high-Z materials or impurities are present, the treatment of laser heating and radiation are highly dependent upon the level of ionization in the plasma and energy which goes into increased ionization.

The laser-plasma heating calculations of McCann (ref. 1) were made with the assumption that the plasma was fully-ionized, but in a separate calculation he showed that the effects due to ionization are, indeed, quite significant. This strong dependence on ionization can be attributed to (1) the actual energy used to increase the level of ionization is a significant fraction of the total energy; (2) most of the dominant physical effects in the plasma are dependent upon the level of ionization in the plasma or the average level of ionization, $\overline{Z}$. These effects include the radiations already mentioned, electron thermal conductivity, and the ion-electron collisional energy exchange; (3) a temperature dependent ionization model would be more accurate than assuming full ionization. One must be careful, however, to use an appropriate model.

For these reasons, the corona model (ref. 2) as used by McCann was incorporated into the calculations of the laser heating as performed by the one-dimensional, Lagrangian coordinate, hydrodynamic code, DULAH. The incorporation of both a temperature-dependent ionization model and the capability to treat a variety of impurity elements has resulted in a new code, DULAH2. Section II exhibits the modifications to DULAH which were necessary to incorporate these capabilities.

Since a knowledge of the optical interactions between the incident laser light and these preformed plasmas would aid in optimizing the laser heating, a two-dimensional, optical, ray-tracing code, RATRACE, was developed to examine several

effects of interest in these plasmas, namely refraction, reflection, and integrated absorption. Some preliminary results of this type of study are presented in section III, and some one-dimensional heating calculations of exploding wires are discussed in section IV.

SECTION II

CORONA MODEL CALCULATIONS OF AVERAGE IONIZATION LEVEL AND ENERGY

The steady-state corona model is an atomic model which assumes that there is a balance between collisional ionization (and excitation) and radiative combination (and spontaneous decay) in the optically thin approximation, i.e., all radiative escapes without further interaction. This model assumes that changes in plasma parameters take place slowly enough for the ion populations to assume their new steady-state values at any instant. Note that in this model the ion population distribution is independent of electron density. The equation governing these ion populations can now be stated as the following:

$$\frac{n(Z)}{n(Z+1)} = 7.87 \times 10^{-9} \{\chi(Z)\}^2 \left\{\frac{\chi(Z)}{kT_e}\right\}^{3/4} \exp\left\{\frac{\chi(Z)}{kT_e}\right\} \tag{1}$$

where $\chi(Z)$ is the total ionization potential to get from a neutral atom to charge state Z,

$$\chi(Z) = \sum_{i=1}^{Z+1} \chi_{g \to i} \tag{2}$$

In the work by McWhirter (ref. 2) the criterion for applicability of this model is given by

$$n_e < 5.6 \times 10^3 (Z+1)^6 T_e^{1/2} \exp\left\{\frac{1.162 \times 10^3 (Z+1)^2}{T_e}\right\} \tag{3}$$

with T_e in degrees Kelvin. Some limiting cases for this model for various values of Z are plotted in figure 1 derived from equation (3).

From equation (1) and the laws of charge neutrality and charge conservation given by

$$n_e = \sum_{i=1}^{Z} Z_i n_i \tag{4}$$

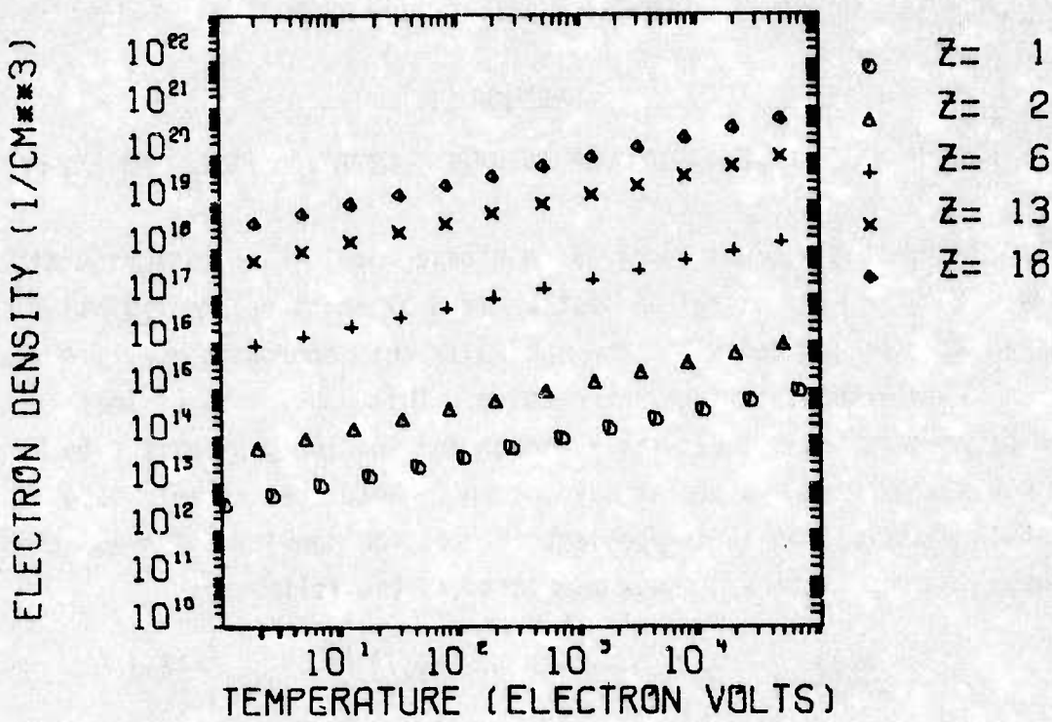

Figure 1. Corona Model Limits for Various Values of Z

the following relationship can be derived for the number density of species i

$$n_i = \frac{n_e \prod_{j=2}^{i} f_j(T_e)}{1 + \sum_{i=2}^{Z} Z_i \prod_{j=2}^{i} f_j(T_e)} \tag{5}$$

where $f_j(T_e)$ is equivalent to $n(Z+1)/n(Z)$ and is given by the inverse of equation (1).

The CORONA program (ref. 1) does not properly calculate the species densities and the average ionization level for materials with $Z \leq 2$. The explicit forms for these cases are the following (with the assumption that a normalized number of electrons are present).

<u>Z = 1</u>

$$n_0 = 1$$

$$n_1 = 1/f_1$$

$$\bar{Z} = f_1/(f_1+1) \tag{6}$$

$\underline{Z = 2}$

$$n_0 = \frac{1}{f_1(1+2f_2)}$$

$$n_1 = \frac{1}{1 + 2f_2}$$

$$n_2 = \frac{f_2}{1 + 2f_2} \tag{6}$$

or

$$\bar{Z} = \left(\frac{1 + 2f_2}{1 + 2f_1}\right) f_1 \tag{7}$$

In both cases, the average ionization energy is given by

$$E_I = \sum_{i=1}^{Z} n_i \; \chi(Z) \tag{8}$$

where $\chi(Z)$ is the total ionization energy required to reach charge state Z and is given by equation (2).

1. CORRECTIONS TO DIFFERENCE SCHEME

The equations governing the ion and electron internal energies, ε_i and ε_e, respectively, are the following:

$$\frac{d\varepsilon_i}{dt} = -P_i \frac{dV}{dt} + Q_{ei} + \frac{T_e}{32 + T_e} \dot{S}_T \tag{9}$$

$$\frac{d\varepsilon_e}{dt} = -P_e \frac{dV}{dt} - Q_{ei} + \overline{\phi K} + \dot{E}_c - \dot{Q}_r + \frac{32}{T_e + 32} \dot{S}_T - E_I \tag{10}$$

where

$P \frac{dV}{dt}$ = energy transferred between internal kinetic energy

Q_{ei} = energy transferred in ion-electron collisions

$\overline{\phi K}$ = energy absorbed from laser by inverse bremsstrahlung

$\dot{E}_c$ = thermal heat condition

$\dot{Q}_r$ = bremsstrahlung radiation

$\frac{T_e}{32 + T_e} \dot{S}_T$ = thermonuclear energy deposited in ions by α's

E_I = average ionization energy

In modifying the above equations to include time-dependent ionization effects, the ionization energy, E_I, must be accounted for as well as using a time-dependent $\overline{Z}$ in the expansion of terms. In some of the above terms it is necessary to derive the correction terms because of a nonzero $\frac{d}{dt}\overline{Z}$; these include the bremsstrahlung radiation terms, the ion-electron collisional exchange term, and the heat conduction term. All of the other terms may be utilized as expounded by Brueckner, et al. (ref. 3) by merely replacing $\overline{Z}$ with a time-varying $\overline{Z}$ instead of assuming full ionization.

Using an implicit difference scheme, the following are used

$$\left.\frac{d\varepsilon_e}{dt}\right|_{t^{n+1/2}} \simeq \frac{\varepsilon_e^{n+1} \quad \varepsilon_e^{n}}{2\Delta t^{n+1/2}} = \frac{W^{n+1/2}}{\Delta t^{n+1}} \tag{11}$$

and

$$\left.\frac{d\varepsilon_i}{dt}\right|_{t^{n+1/2}} \simeq \frac{\varepsilon_i^{n+1} - \varepsilon_i^{n}}{2\Delta t^{n+1/2}} = \frac{U^{n+1/2}}{\Delta t^{n+1}} \tag{12}$$

Using the quantities from the nth time step (denoted by n superscript) for the appropriate zone or boundary (denoted by half-integral and integral subscripts, respectively), the appropriate quantities can be calculated at time $t^{n+1} = t^n + \Delta t^{n+1}$.

The corrections which must be made and the resulting difference equations are as follows:

a. Bremsstrahlung Radiation Term

The bremsstrahlung radiation is given by

$$\dot{Q}_r = C_r' \, N_i^2 \, \overline{Z}^3 \left\{\frac{A\varepsilon_e}{\overline{Z}}\right\}^{1/2} \tag{13}$$

or

$$\dot{Q}_r = C_r' \, N_i \, \bar{Z}^{5/2} \, A\varepsilon_e^{1/2} \tag{14}$$

Noting that N_i is not constant in time because the volume is allowed to change although the total number of ions considered is held constant, and differentiating equation (14) yields

$$\ddot{Q}_r = \dot{Q}_r \left\{ \frac{2\dot{N}_i}{N_i} + \frac{1}{2}\frac{\dot{\varepsilon}_e}{\varepsilon_e} + \frac{5}{2}\frac{\dot{\bar{Z}}}{\bar{Z}} \right\} \tag{15}$$

Therefore, applying the same differencing as in equations (11) and (12),

$$\dot{Q}_r^{\,n+1/2} = \dot{Q}_r^{\,n} \left\{ 1 + \frac{\Delta N_i^{\,n+1/2}}{N_i^{\,n}} + \frac{5}{4}\frac{\Delta \bar{Z}^{n+1/2}}{\bar{Z}^n} + \frac{1}{4}\frac{W^{n+1/2}}{\varepsilon_e^{\,n}} \right\} \tag{16}$$

The middle two terms are terms not considered in the previous work (ref. 3).

b. Thermal Conduction Term

The thermal conduction term is of the following form:

$$\dot{E}_c = \frac{2}{7} \chi_0' \frac{\partial}{\partial m} \left\{ \frac{R^{\alpha-1}}{\bar{Z} \, \ell n \, \Lambda} \frac{\partial}{\partial R} \frac{AG}{\bar{Z}}^{7/2} \right\} \tag{17}$$

The spatial centering of this equation as done in the original work (ref. 3) is correct. However, the implicit approximation that was used must be changed. Using the type relationship in equation (11) results in:

$$\left(\frac{A\varepsilon_e^{\,n+1}}{\bar{Z}^{n+1}} \right)^{7/2} \simeq \left(1 - \frac{7}{4} \frac{\Delta \bar{Z}^n}{\bar{Z}^n} \right) \left(\frac{A\varepsilon_e^{\,n}}{\bar{Z}^n} \right)^{7/2} + \frac{7}{4} \left(\frac{A\varepsilon_e^{\,n}}{\bar{Z}^n} \right)^{5/2} \left(\frac{A}{\bar{Z}^n} \right) W^{n+1/2} \tag{18}$$

This replaces the approximation

$$\left(\varepsilon_e^{\,n+1} \right)^{7/2} \simeq \left(\varepsilon_e^{\,n} \right)^{7/2} + \frac{7}{4} \left(\varepsilon_e^{\,n} \right)^{5/2} W^{n+1/2} \tag{19}$$

The differencing of equation (17) yields.

$$\left(\dot{E}_c\right)_{j-\frac{1}{2}}^{n+\frac{1}{2}} = \frac{2}{7}\frac{X_0'}{m_{j-\frac{1}{2}}}\left\{R_j^{n+\frac{1}{2}\alpha-1}\frac{\left[\left(A\varepsilon_e/\overline{Z}\right)^{7/2}\right]_{j-\frac{1}{2}}^{n+\frac{1}{2}} - \left[\left(A\varepsilon_e/\overline{Z}\right)^{7/2}\right]_{j-\frac{1}{2}}^{n+\frac{1}{2}}}{\frac{1}{2}\left[\left(\overline{Z}\ \ell n\ \Lambda\right)_{j-\frac{1}{2}}\left(R_j^{n+\frac{1}{2}} - R_{j-1}^{n+\frac{1}{2}}\right) + \left(\overline{Z}\ \ell n\ \Lambda\right)_{j+\frac{1}{2}}\left(R_{j+1}^{n+\frac{1}{2}} - R_j^{n+\frac{1}{2}}\right)\right]}\right.$$

$$\left. -R_{j-1}^{n+\frac{1}{2}\ \alpha-1}\frac{\left[\left(A\varepsilon_e/\overline{Z}\right)^{7/2}\right]_{j-\frac{1}{2}}^{n+\frac{1}{2}} - \left[\left(A\varepsilon_e/\overline{Z}\right)^{7/2}\right]_{j-3/2}^{n+\frac{1}{2}}}{\frac{1}{2}\left[\left(\overline{Z}\ \ell n\ \Lambda\right)_{j-3/2}\left(R_{j-1}^{n+\frac{1}{2}} - R_{j-2}^{n+\frac{1}{2}}\right) + \left(\overline{Z}\ \ell n\ \Lambda\right)_{j-\frac{1}{2}}\left(R_j^{n+\frac{1}{2}} - R_{j-1}^{n+\frac{1}{2}}\right)\right]}\right\} \quad (20)$$

Upon proper substitution for $\left(\varepsilon_e^{n+1}\right)^{7/2}$ as given in equation (19), this form is correct.

2. ION-ELECTRON COLLISIONAL EXCHANGE

The ion-electron energy exchange term which appears in equations (9) and (10) is given by (ref. 3) as

$$Q_{ei} = \frac{N_e}{\tau_0'\ \varepsilon_e^{3/2}}\left(\frac{\varepsilon_e}{\overline{Z}} - \varepsilon_i\right) \quad (21)$$

where

$$\tau_0' = 1.83 \times 10^{-10}\ A\left(\frac{A}{\overline{Z}}\right)^{3/2}\frac{1}{\overline{Z}^2\ \ell n\ \Lambda} \quad (22)$$

Substituting

$$\tau_0' = \tau_0''\frac{1}{\overline{Z}^{7/2}} \quad (23)$$

into equation (21) makes τ_0'' independent of time and

$$Q_{ei} = \frac{\overline{Z}^{\,7/2}}{\tau_0''}\left\{\frac{N_e}{\varepsilon_e^{3/2}}\left(\frac{\varepsilon_e}{\overline{Z}} - \varepsilon_i\right)\right\} \quad (24)$$

Taking the time derivative of equation (24) yields

$$\dot{Q}_{ei} = \frac{\partial Q_{ei}}{\partial \varepsilon_e}\frac{\partial \varepsilon_e}{\partial t} + \frac{\partial Q_{ei}}{\partial \varepsilon_i}\frac{\partial \varepsilon_i}{\partial t} + \frac{\partial Q_{ei}}{\partial N_e}\frac{\partial N_e}{\partial t} + \frac{\partial Q_{ei}}{\partial \bar{Z}}\frac{\partial \bar{Z}}{\partial t}$$

Evaluating these partial derivatives yields

$$\dot{Q}_{ei} = \frac{\bar{Z}^{7/2}\, N_e}{\tau_0''\, \varepsilon_e^{\,3/2}} \left\{ \frac{1}{2}\left(3\,\frac{\varepsilon_i}{\varepsilon_e} - \frac{1}{\bar{Z}}\right)\dot{\varepsilon}_e - \frac{\dot{\varepsilon}_i}{\varepsilon_i} + \frac{\dot{N}_e}{N_e}\left(\frac{\varepsilon_e}{\bar{Z}} - \varepsilon_i\right) \right.$$

$$\left. + \frac{1}{2}\left(5\,\frac{\varepsilon_e}{\bar{Z}^2} - 7\,\frac{\varepsilon_i}{\bar{Z}}\right)\dot{\bar{Z}} \right\} \qquad (26)$$

Where the last term is a term which does not appear in the original calculations and must be integrated and included in the calculation of $Q_{ei}^{n+\frac{1}{2}}$.

SECTION III

RAY TRACING STUDIES ON EXPLOSING WIRES

1. OPTICS

The ray tracing of a laser beam through a plasma is accomplished by first establishing a two-dimensional, rectangular coordinate grid which sets up a plane of cells (figure 2). RATRACE (ref. 4) accomplishes the propagation of a single plane-wave ray through this grid by the application of plane-wave optics at the cell boundaries. This includes the law of refraction at a plane surface

$$n_i \sin \psi_1 = n_2 \sin \psi_2 \tag{27}$$

and the law of reflection

$$\psi_c = \sin^{-1}\left(\frac{n_2}{n_1}\right) \tag{28}$$

where n is the index of refraction and ψ is the angle of incidence with respect to the normal; the subscripts 1 and 2 refer to the values of these quantities on the respective sides of the interface. The ray is propagated across the cell in a straight line until the cell boundary is encountered. Optical effects are calculated at the cell interface, and the ray is propagated across the appropriate cell. This process continues until the system boundary is encountered. At this point the trace of the ray in the system of interest is plotted on microfilm.

For this calculation, the index of refraction is defined from the electron number density by

$$n \cong \left(1 - \frac{N_e}{N_e{}^c}\right)^{1/2} \tag{29}$$

where N_e (cm^{-3}) is the electron density in the cell and $N_e{}^c$ (cm^{-3}) is the critical electron density which is defined as the density at which the plasma frequency, ν_p, equals the laser frequency, ν_L,

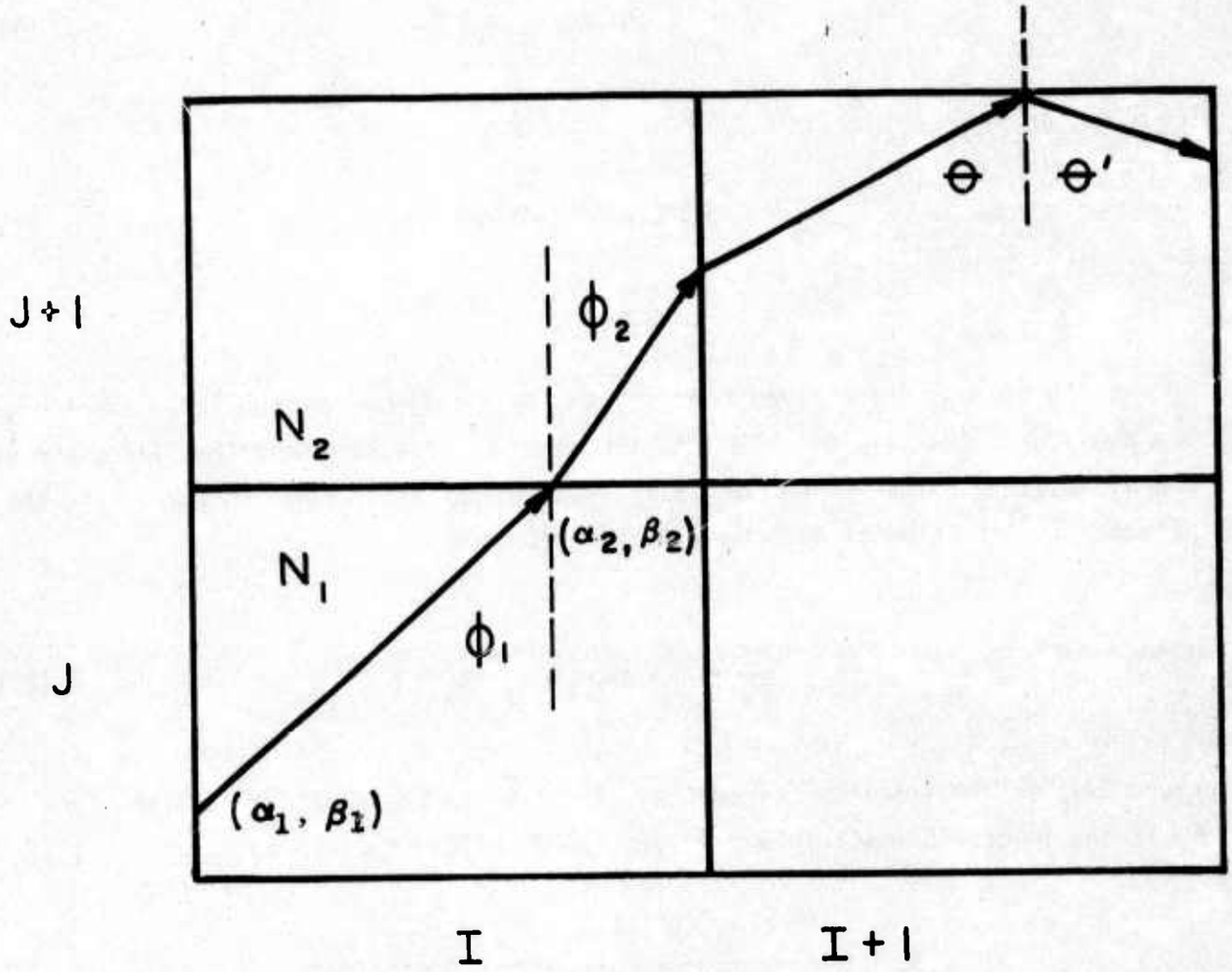

Figure 2. Typical Cell Configuration and Ray Tracing Progression

$$N_e^c = \frac{\left(2\pi\ \nu_L\right)^2\ \varepsilon_0\ me}{q^2} \tag{30}$$

(ref. 5), where the plasma frequency is given by

$$\nu p = \frac{1}{2\pi}\ (q^2\ N_e/\varepsilon_0\ m_e)^{1/2} \tag{31}$$

(ref. 1) or by

$$\nu_p = 8.98 \times 10^3\ N_e^{1/2}(\sec^{-1}) \tag{31a}$$

2. ABSORPTION

In the plasmas under investigation, the path followed by the laser light does not fully or adequately describe the interaction. Another important indicator of the interaction is the amount of laser light which is absorbed in traversing the plasma. The fraction of absorbed light is given by

$$1 - \frac{I}{I_o} = 1 - \exp\left(- \int K_a dx\right) \tag{32}$$

where I/I_o is the fraction transmitted, $1 - I/I_o$ is the fraction absorbed, and K_a is the inverse bremsstrahlung absorption coefficient given by

$$K_a = \frac{16\ \bar{Z}\ N_e^2\ q^6\ \ell n\ \Lambda}{3c\ \nu_L^2\ \left(2m_e\ kT_e\right)^{3/2}}\ \frac{1}{\left(1 - \nu_p^2/\nu_L^2\right)^{1/2}} \tag{33}$$

(ref. 6), or upon substitution by

$$K_a = \frac{1.56 \times 10^{-8}\ \bar{Z}\ N_e^2\ \ell n\ \Lambda}{\nu_L^2\ \left(kT_e\right)^{3/2}}\ \frac{1}{\left(1 - \nu_p^2/\nu_L^2\right)^{1/2}} \tag{33a}$$

For use in RATRACE the absorption integral is approximated by the finite summation

$$\int K_a \, d_x \simeq \sum_{\substack{i \text{ for} \\ \text{all} \\ \text{cells}}} K_{ai} \, \Delta r_i \tag{34}$$

where K_{ai} is the appropriate absorption coefficient for cell i, and Δr_i is the distance travelled across the cell.

The combination of the optical path traversed by the ray and the amount of energy absorbed during this traversal is used to characterize the interaction of the laser and the plasma.

3. APPLICATION TO EXPLODING WIRE STUDIES

Exploding wires produce plasmas which can be laser heated. In treating the heating of these plasmas, the inverse bremsstrahlung mechanism of heating is assumed. The absorption coefficient for this mechanism is functionally dependent upon temperature, electron density, ionization level, and laser frequency. The optical effects as well as the effects of the above parameters can be simulated using the RATRACE code.

The density profiles used in this work are analytical fits to the data obtained on aluminum exploding wires by holographic interferometry (ref. 7), where the electron density distributions were found to be almost exponentially decreasing with distance from the center of the wire.

Experimental studies of the heating of exploding wire plasmas are to be conducted using one wire and two parallel wires. Theoretical studies of these configurations have been made using the RATRACE code and have yielded some interesting results which are portrayed in figures 3 through 8. In these figures the contours of electron density are all the same: the minimum is 1.0×10^{17} cm^{-3}, the maximum 7.8×10^{18} cm^{-3}, and they are spaced 1.1×10^{18} cm^{-3} apart.

Simulation of the laser beam incident upon one wire showed a large amount of scattered light and high absorption for the CO_2 laser, $\lambda = 10.6$ μm (figure 3), and essentially no scattered light and much less absorption for the ruby laser,

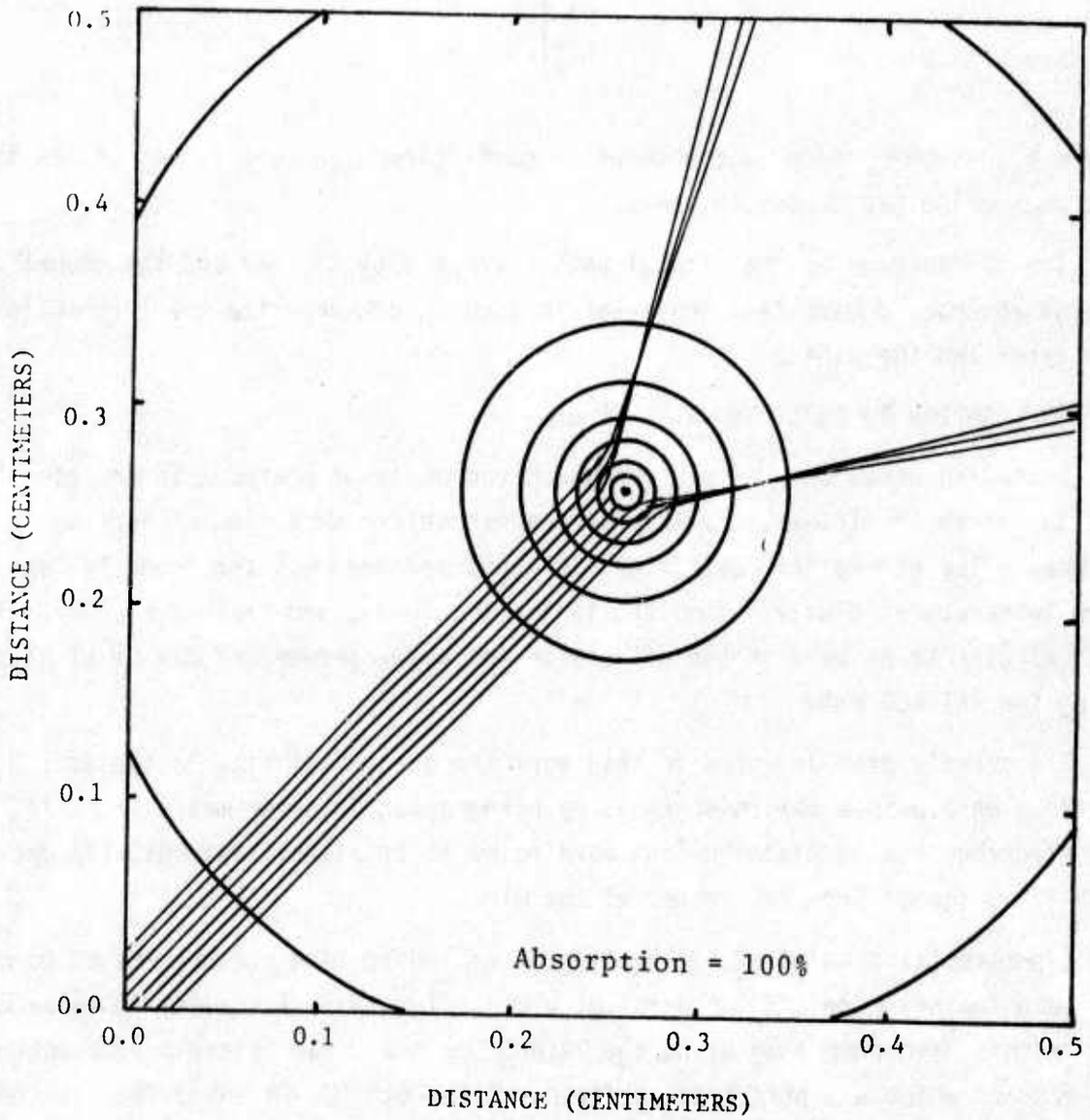

Figure 3. Collimated CO_2 Laser Incident on One Wire

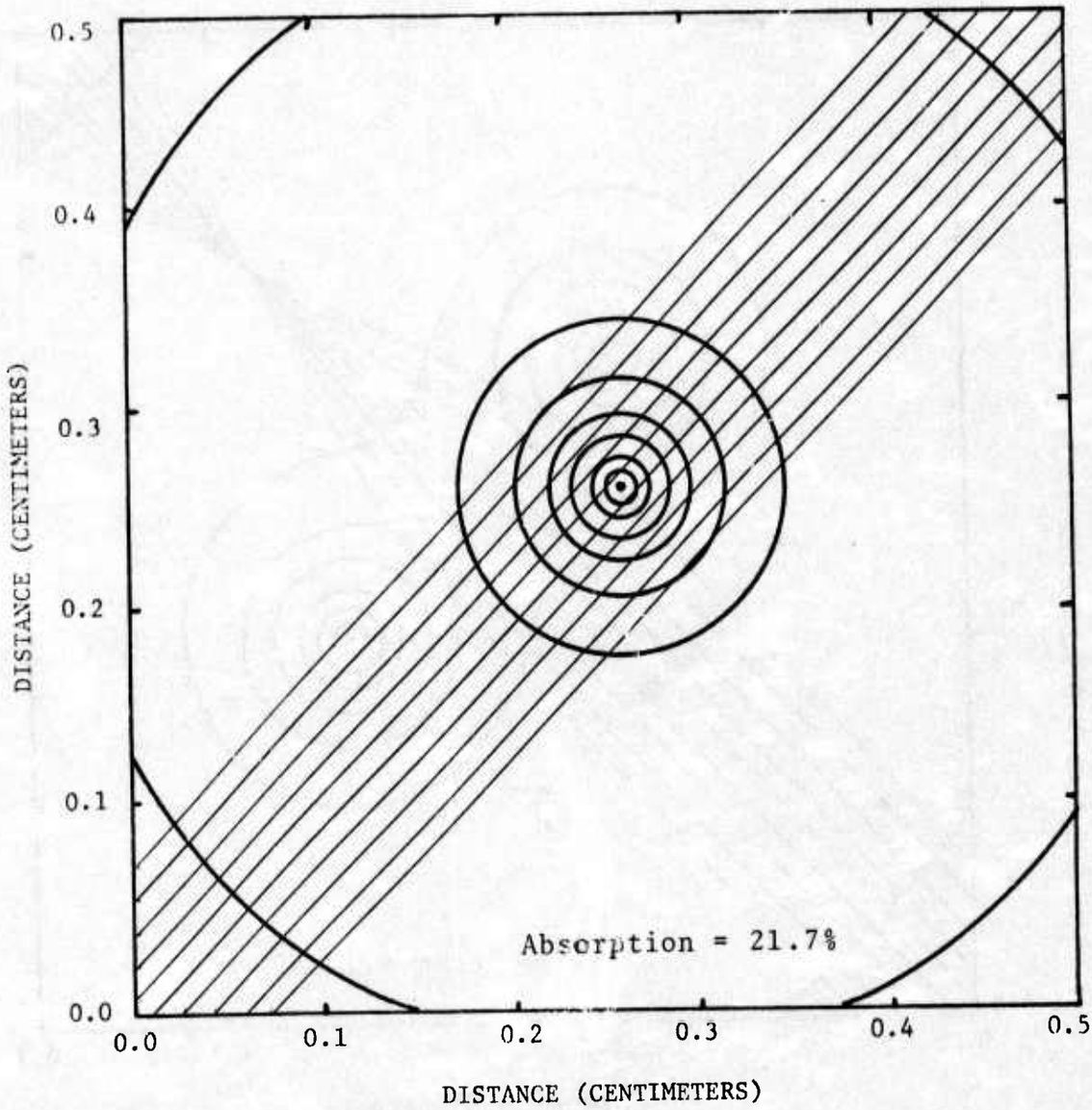

Figure 4. Collimated Ruby Laser Incident on One Wire

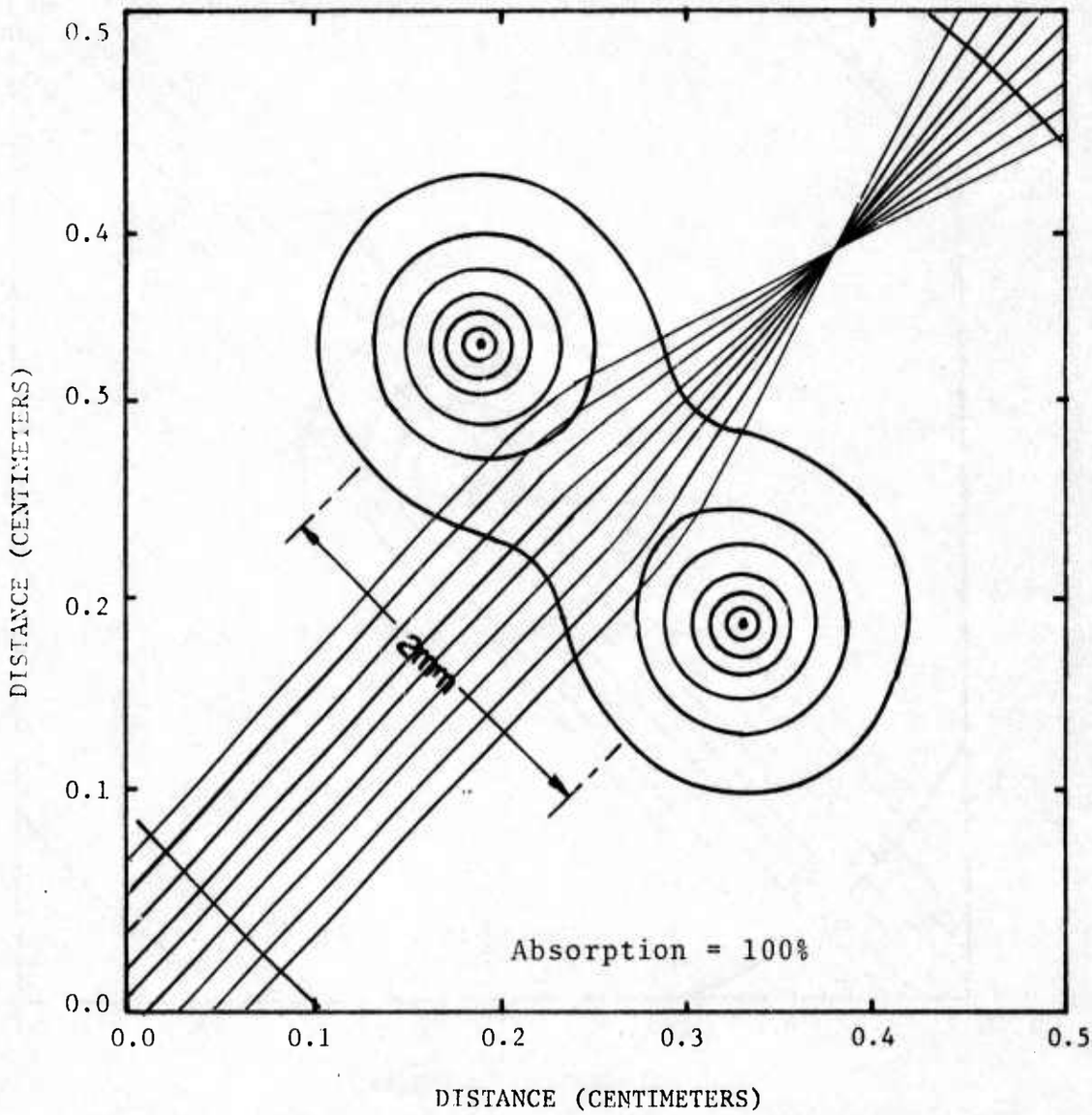

Figure 5. Collimated CO_2 Laser Incident on Two Wires

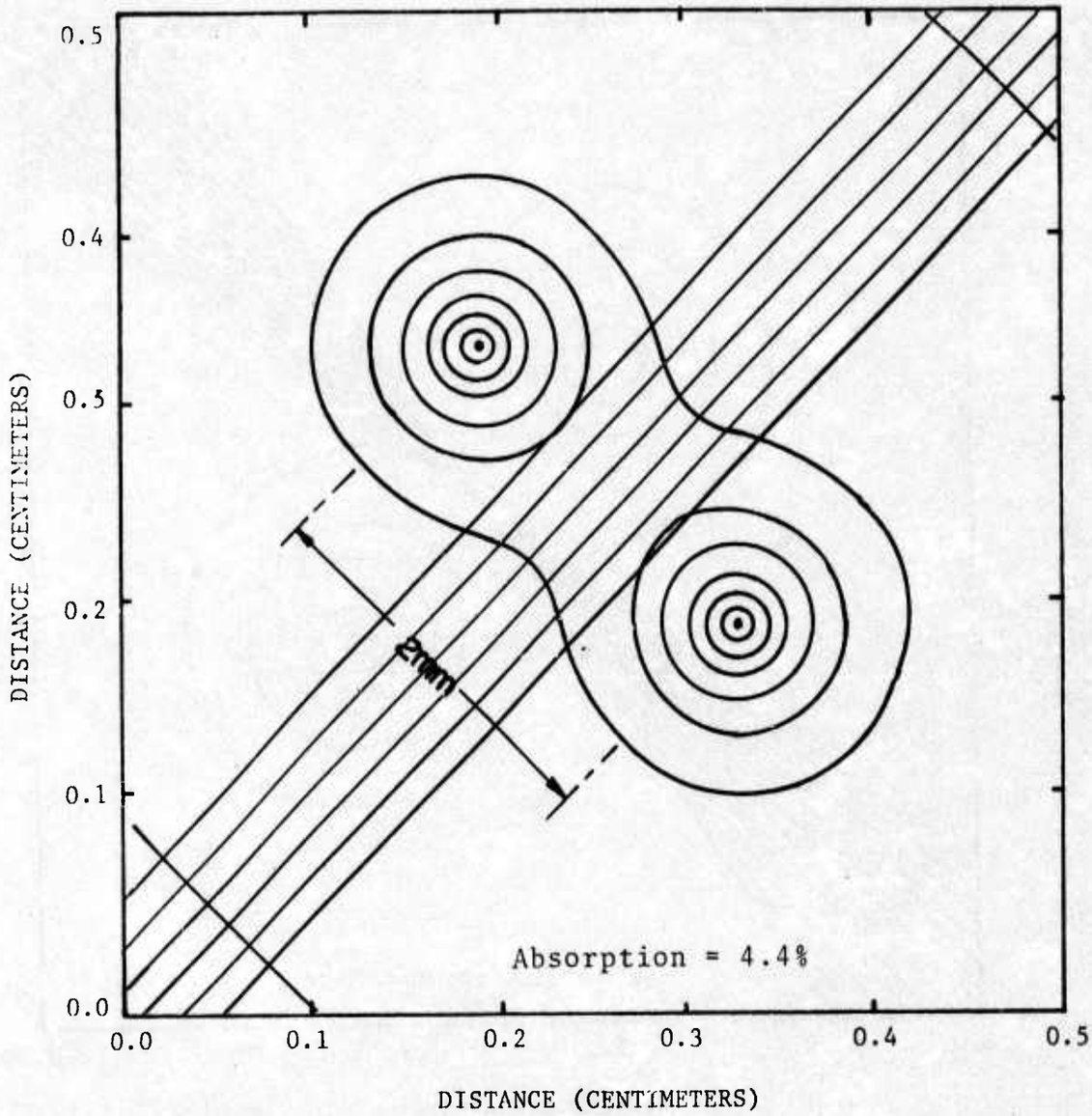

Figure 6. Collimated Ruby Laser Incident on Two Wires

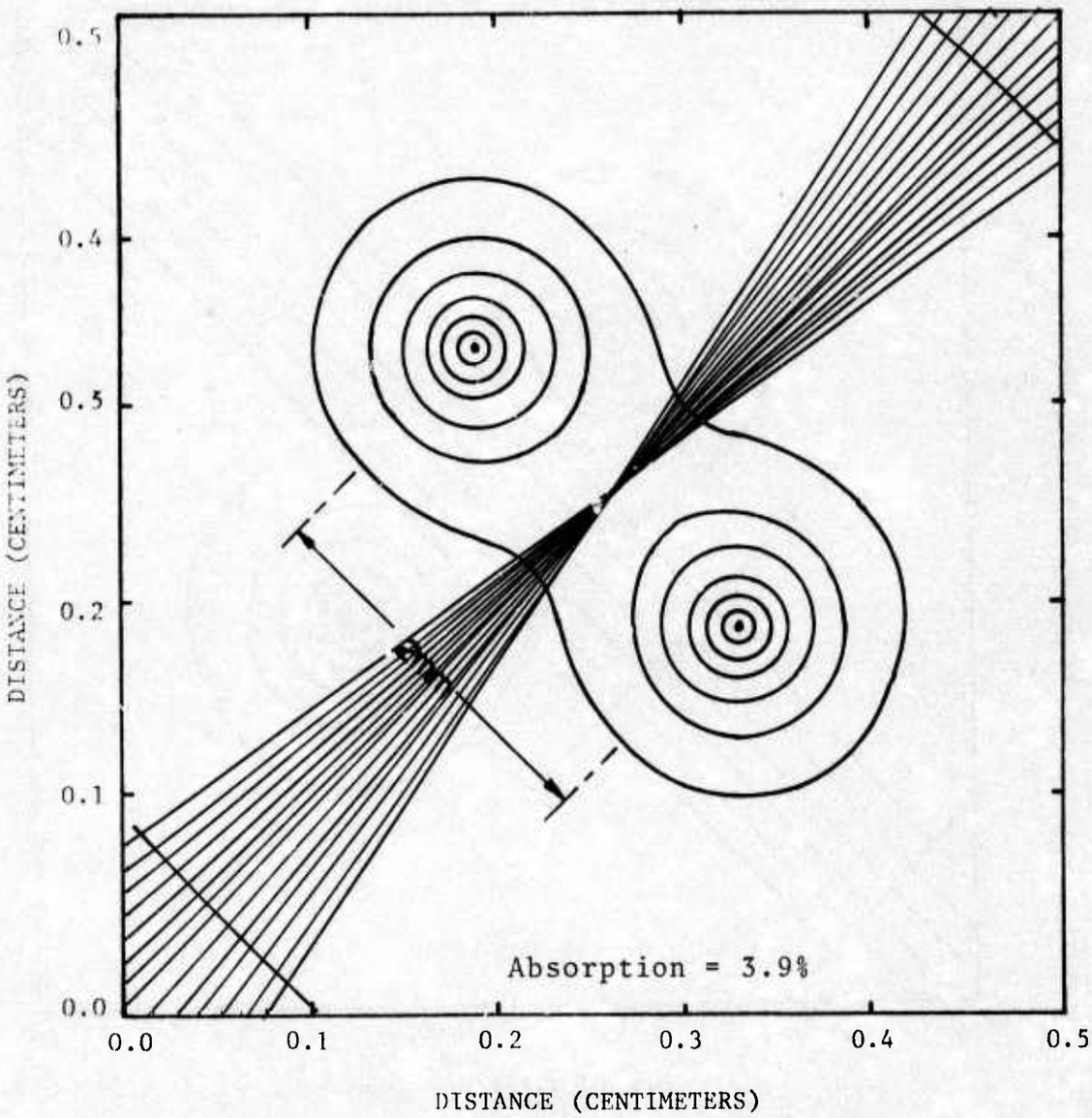

Figure 7. Focused Ruby Laser Incident on Two Wires

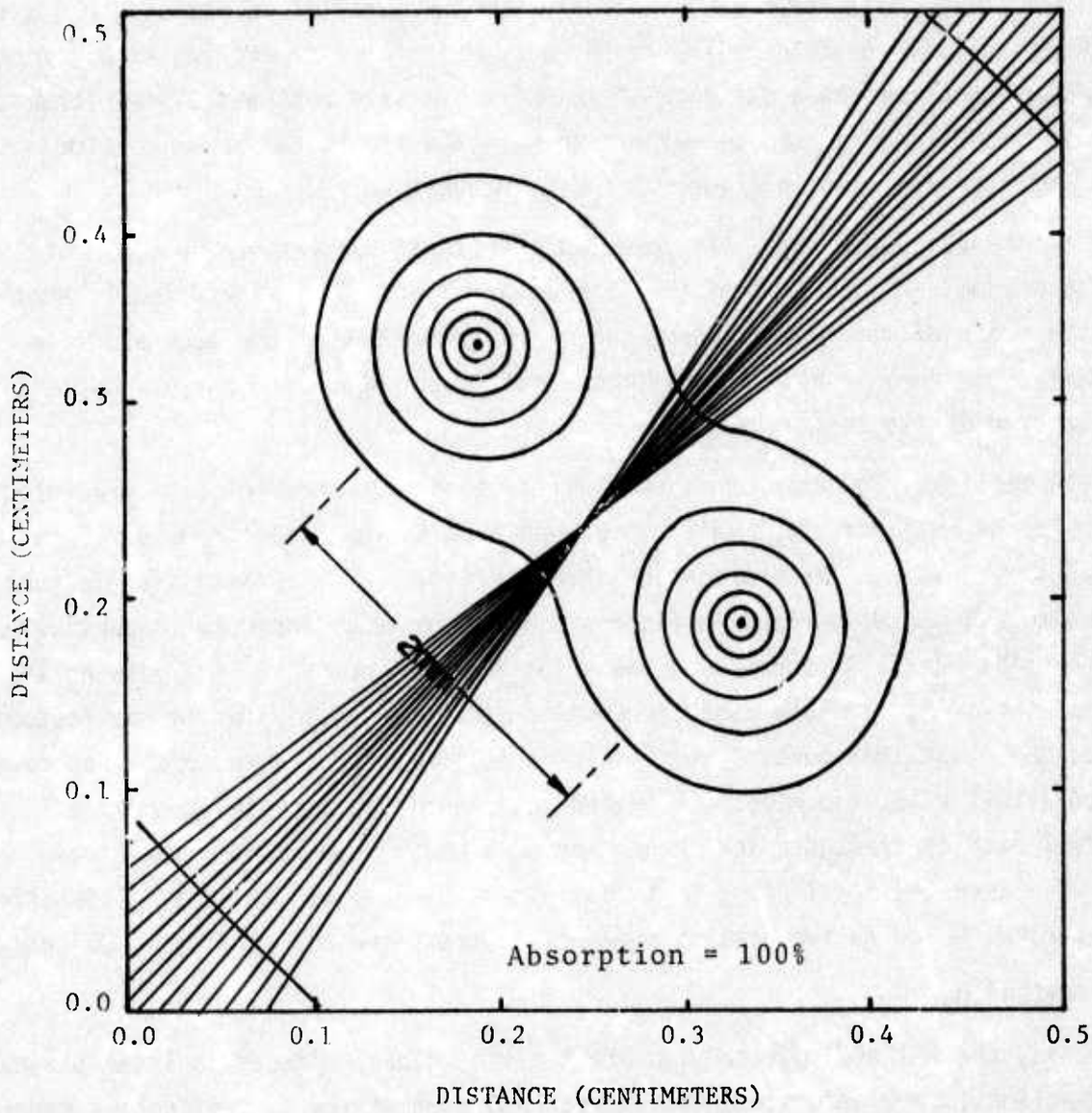

Figure 8. Focused CO_2 Laser Incident on Two Wires

$\lambda = 0.6943\ \mu$ (figure 4). This is to be expected because of the proportionality of the absorption coefficient to the square of the wavelength. The larger refractive effects occur for the CO_2 case since the electron density is near the critical density for CO_2 (1×10^{19} cm^{-3}), whereas in the ruby case the electron density is far below the critical density for ruby (2.33×10^{21} cm^{-3}).

Simulation of a laser beam incident upon two parallel exploding wires used an electron density profile consisting of a superposition of the two single wire profiles separated by a distance of (2 mm). The same collimated laser beams, CO_2 and ruby, used in the one-wire case were applied to the two-wire simulation. The results are shown in figures 5 and 6, respectively.

In the CO_2 laser case, the focusing effects of the two-wire profile are quite predominant. The wires function as a focusing lens with a focal length on the order of the separation of the wires (2 mm). With the same electron density, the ruby laser is transmitted unaffected except for the 4.4 percent absorption of the beam intensity.

In reality, the laser beams which will be used in the exploding wire studies will not be collimated but will be focused from a 2-cm diameter by a 7.5-cm focal length lens. The propagation characteristics of this beam are employed in the simulations represented in figures 7 and 8 for ruby and CO_2, respectively. The beam is initially focused on the point which bisects the line joining the two wire centers. In the ruby case the position of this focal point is unaffected. Note, too, that this focused case yields a somewhat reduced absorption as compared with the corresponding collimated case. This is because the beam's optical path is through a less dense region when focused between the wires. For the CO_2 laser the focal point is moved somewhat nearer to the lens. This effect is expected based on the results shown in figure 5 for the collimated CO_2 beam.

4. CONCLUSIONS

Using the RATRACE code to simulate two-dimensional effects in laser-plasma interactions, some understanding has been achieved of the most effective manner in which to heat a preformed plasma given its configuration and some basic assumptions about the absorption mechanism. From the tests which have been run to date, the CO_2 laser incident upon two wires looks the most promising in terms of the amount of energy which can be deposited in the plasma by the beam. From the predicted absorption and light paths, some important points of comparison with

diagnostic techniques have been established. This should aid in an understanding of these interactions when these diagnostics can be performed.

SECTION IV

INITIATION AND LASER HEATING OF EXPLODING WIRE PLASMAS

In the consideration of laser heating of exploding wire plasmas, a number of important questions arise which must be considered:

(1) In the initiation phase of exploding a wire with stored energy in a capacitor bank, what are the physical properties of the wire as a function of time--phase, temperature, diameter, and density?

(2) What are the spatial variations of these parameters?

(3) Given the shape, power, and duration of the laser pulse, what is the best time to begin heating the plasma? Some parametric questions which may also be of interest are the following: (1) what density gradient enhances the heating of a preformed plasma most effectively, and (2) how does the laser heating scale with pulse length and energy?

The present work is concerned with some parametric, one-dimensional studies of the laser heating of aluminum exploding-wire plasmas with a CO_2 laser. This study was conducted in two phases:

(1) Using the one-dimensional magnetohydrodynamic code, MAGPIE, (ref. 8), consideration was given to the initiation of the wire plasma by the capacitor bank. The bank used in these studies has the properties which are listed in table 1. Given these parameters for the capacitor bank, the initiation of wires of three different diameters was studied to determine what conditions could be generated for laser heating.

(2) Given these initial conditions for heating, a one-dimensional laser-hydrodynamics code, DULAH2, was applied to determine what heating could be expected. This code was also used to look at the dependence of heating, upon laser pulse shape and power.

1. EXPLODING WIRE INITIATION

Using the one-dimensional magnetohydrodynamics code, MAGPIE, the initiation of exploding wires of various diameters was studied. These studies assumed the parameters for the stored energy capacitor bank that are listed in table 1. The

Table 1

CAPACITOR BANK PARAMETERS USED
IN INITIATION STUDIES

Capacitance	0.75 microfarads
Resistance	0.29 ohms
Inductance	1.29 microhenries
Voltage	15 kilovolts
Stored Energy	85 joules

three exploding wires considered are aluminum wires of 2.0-cm length with diameter of 1, 2, and 5 mils.

Of obvious importance and interest in this type of calculation is the equation of state used for the wire. The equation of state used in these calculations for aluminum is a three-phase equation of state (liquid, gas, plasma) in empirical form. Thus, the solid-to-liquid phase transition is ignored for the purposes of this calculation. The solid-liquid transition should occur at 0.08 electron volts with a specific heat of 0.215 calorie/gram. For a 2.0-cm, 5-mil diameter wire, the phase change requires approximately 3.5 millijoules of energy. In light of the parameters of the bank used in these studies, this phase transition is of little importance; ignoring it at this point is not significant.

The intent of this phase of the study is to determine what are the best conditions under which to produce an exploding wire plasma if the constraints of the capacitor bank are as already described. The first major consideration in forming a target for laser interaction is that the target, if possible, be in the plasma state. By examining the current through the wire, as a function of time, the state of the plasma should be evident to some degree. The current traces shown in figure 9 are those for the three cases which will be considered. The dip which occurs in the current is attributed to the phase transition from the liquid to the gas. Several important comparison can be made: (1) the larger diameter wires require more current to drive the phase transition; (2) the larger the wire the later in time that the phase transition occurs; (3) the 5-mil diameter wire appears to be the largest wire that this bank will drive across the liquid-gas phase transition; (4) the current rise, point of maximum current, and fall off of the current all occur on approximately the same time scales regardless of

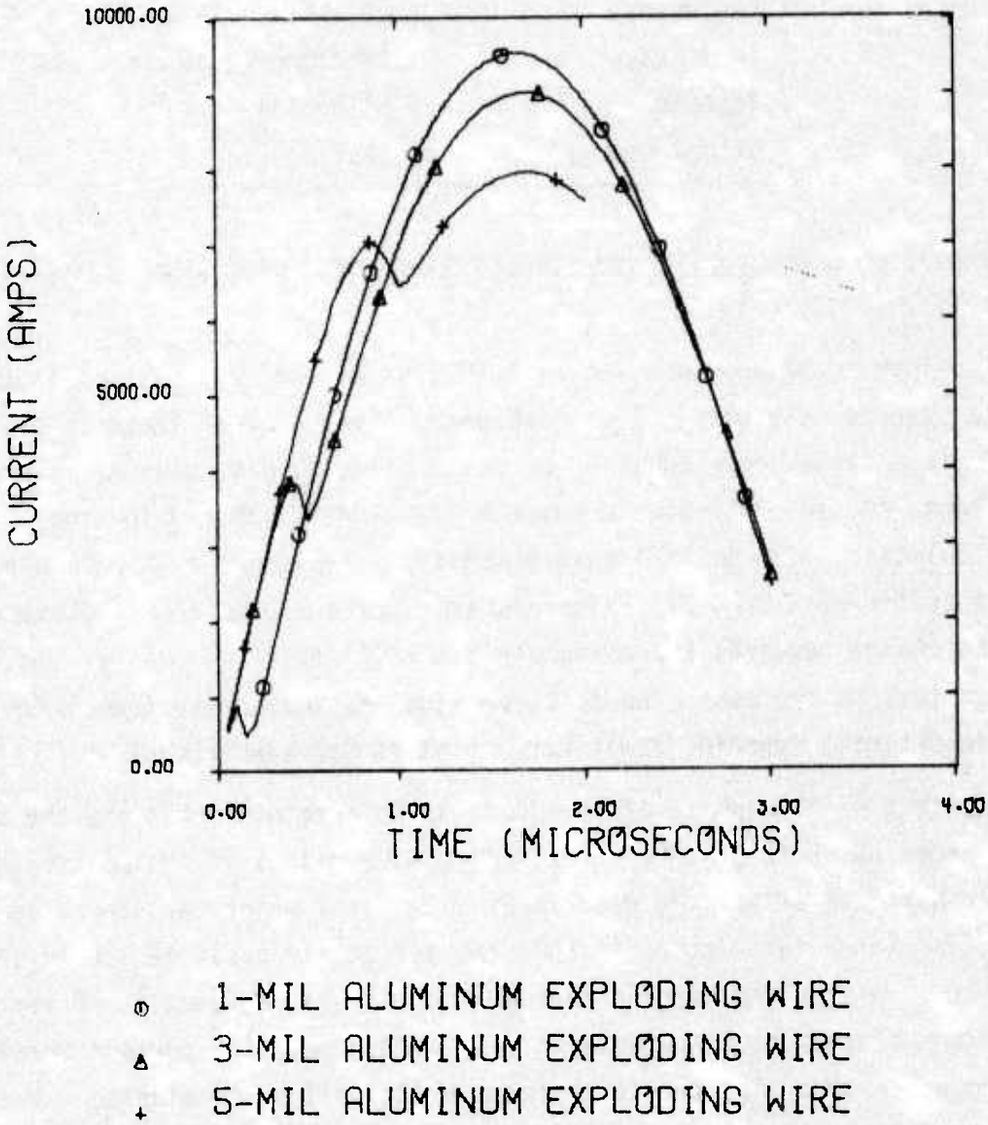

Figure 9. Exploding Wire Current Traces for 1, 3, and 5-mil Aluminum Wires

the wire size (this is with the exception of the current change occurring at the phase change). Thus it appears that the plasma parameters in this case do not significantly modify the parameters of the entire circuit.

The purpose of making these initiation studies is to determine the optimum conditions for laser heating of an exploding wire plasma. Some other indications of the state of the wire which will provide useful information are the wire radius as a function of time and the temperature as a function of time. These are shown in figures 10 and 11, respectively. Both of these figures show some relationships which at first seem strange. There is obviously no simple scaling of these parameters from one wire size to another. Examining figure 10 in detail shows that the wires start expanding at increasingly later times as the wire size increases. This corresponds to the fact that the liquid-gas phase change occurs later in time as seen in the current traces. Immediately after the phase transition, all wires expand outward with approximately the same initial velocity (indicated by the constant and equal sloping lines of the spatial position versus time plot). In the case of the 3-mil and 5-mil wires this expansion expansion continues at constant velocity. However, in the 1-mil case, the expansion velocity. However, in the 1-mil case, the expansion velocity is reduced at about 0.7 microsecond. At this point the magnetic pressure has increased and is confining the expanding plasma.

In examining the temperature versus time plots in figure 11, several different situations exist as in the case of the plasma outer radius. Here there is no simple scaling relationship between the temperature reached and the wire diameter. By comparison with figure 10 it appears that the maximum temperature for each wire is reached shortly after the initial expansion of the wire begins. This corresponds, too, with the transition point of gas to plasma. A strange point is that the maximum temperature reached by the 3-mil wire is higher than the maximum temperature reached by either the 1- or 5-mil wires. It appears that the 1-mil wire has so little mass that it is blown apart by the particle pressure before much ohmic heating can occur and raise the temperature. The 3-mil wire is held together longer and heated more. The 5-mil wire then contains so much mass that the liquid-gas phase transition is barely driven before the point of maximum current, thus allowing very little time after the phase transition for heating to occur and the temperature to rise. The highest temperature is not the ideal case for laser heating; recall that the inverse bremsstrahlung absorption coefficient goes as $T_e^{-3/2}$. Thus increased temperature is an adverse

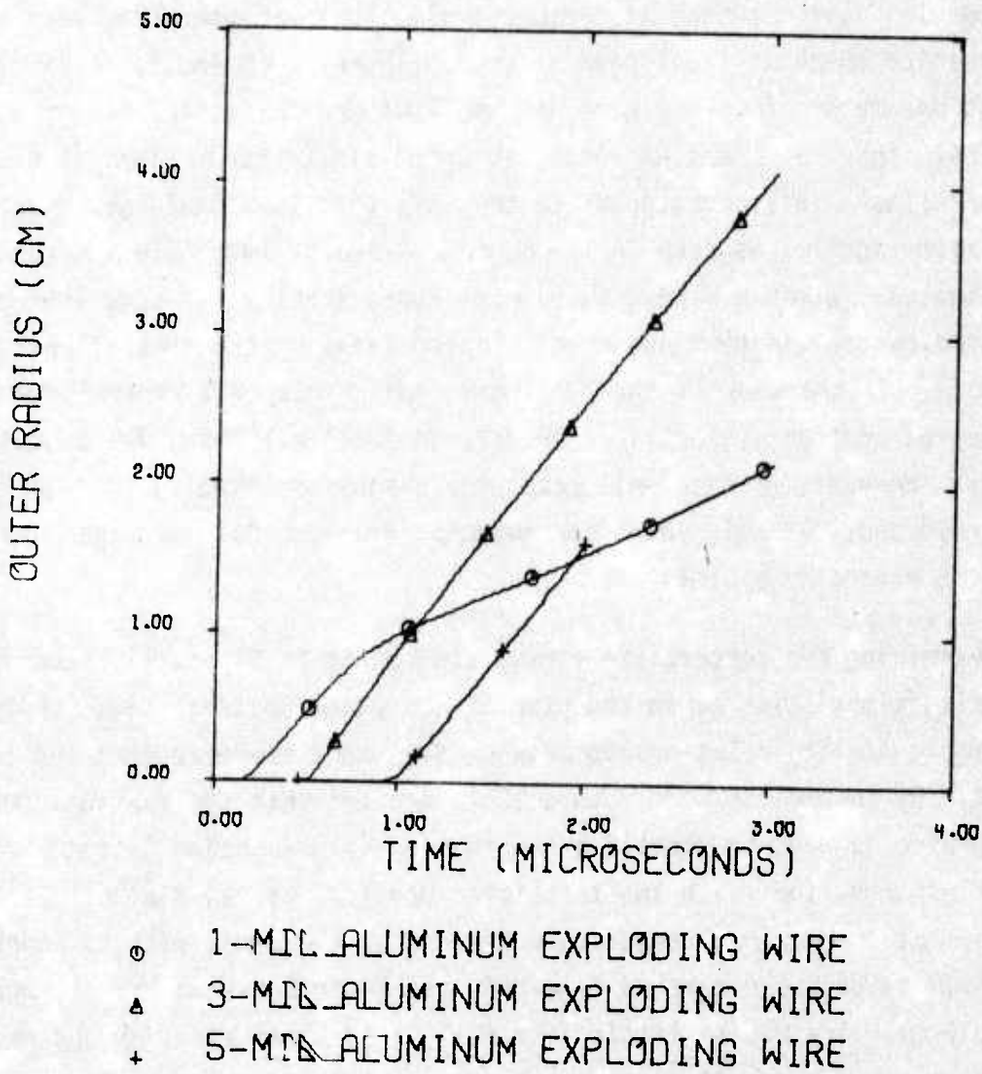

Figure 10. Outer Radius Versus Time for Aluminum Exploding Wires

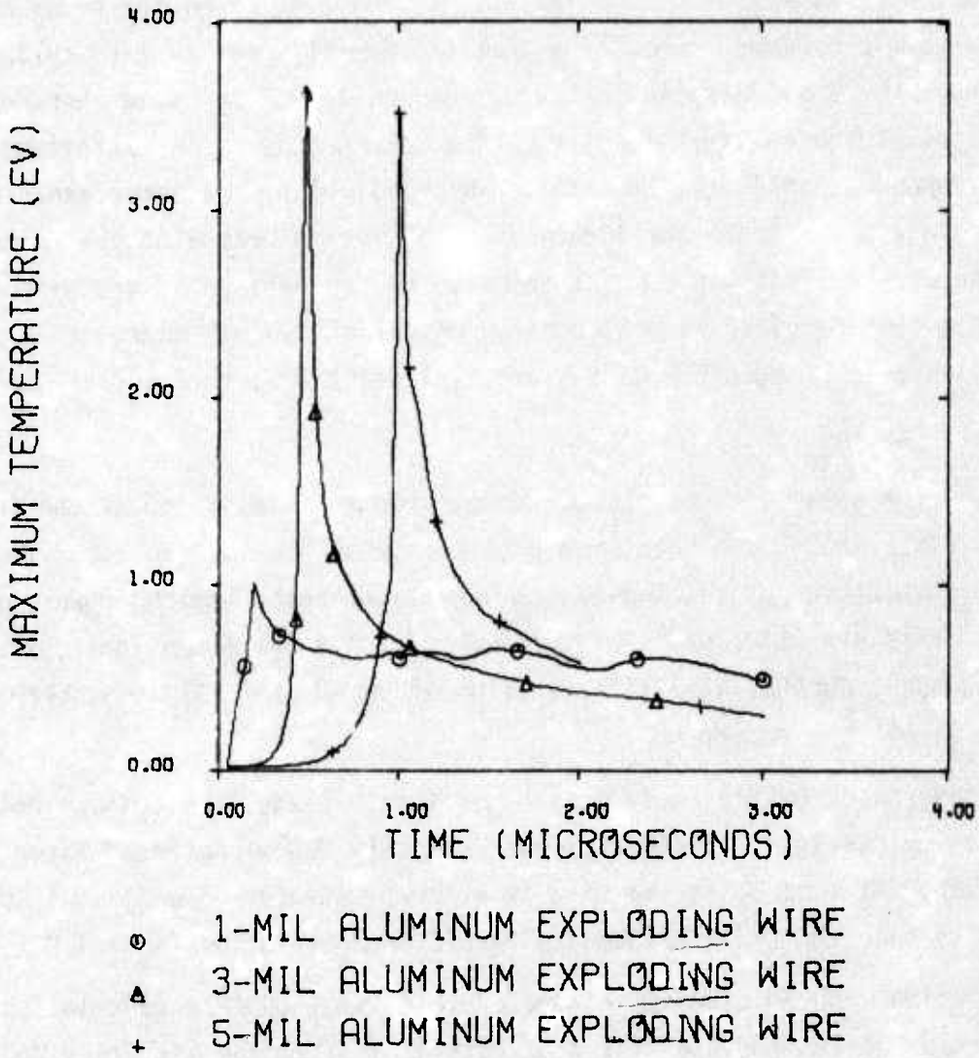

Figure 11. Maximum Temperature Versus Time for Aluminum Exploding Wires

effect for laser heating since the absorption coefficient goes as N_e^2, for N_e less than the critical density. Thus it is important to hit the plasma as close to the critical density in time as possible, even using the laser's leading pulse to help form the plasma into a good heating configuration. It is convenient in this case that the plasma has expanded to reach its critical density long after the maximum temperature is reached; at this point the plasma has cooled off and the absorption coefficient is somewhat increased. The expansion velocity for the 3-mil wire as measured from the plot is found to be on the order of 1.5 centimeter/microsecond. Recalling that the density goes as $1/r^2$ cylindrical geometry), the 3-mil wire would have to expand to 0.3-cm radius before the density is at the critical density. This corresponds to an expansion time of 0.2 microseconds after the transition which allows hydrodynamic expansion to occur. This seems to be the ideal point in time to heat with the laser. For the case of the 3-mil wire, which seems to be the optimum of the wire considered, the lapse time required to meet optimum conditions is 0.8 microsecond after initiation of the capacitor bank which explodes the wire.

2. LASER HEATING

Given the parameters of the preformed plasma as indicated in the initiation phase of this study, the problem now becomes what heating can occur from a CO_2 laser and what kind of scaling exists with laser pulse length, power, and total energy. This parameter study was conducted with a one-dimensional, laser hydrodynamics code, DULAH2, a modified version of DULAH (ref. 3) as described in section II of this report.

As discussed qualitatively in the initiation phase, the optimum heating situation exists in the 3-mil wire approximately 0.8 microsecond after bank initiation. At this point the wire is a low-temperature plasma (0.5 to 1.0 ev) of density near the critical density for 10.6-μm radiation ($N_e = 1.0 \times 10^{19}$).

Beginning with an aluminum plasma of this type, DULAH 2 calculations were made with a CO_2 laser pulse like that obtainable from the Air Force Weapons Laboratory (AFWL) cold-cathode electron beam-sustained CO_2 laser (ref. 9). This laser typically has a gain-switched pulse of 50 to 80 nanoseconds and 50 to 100 joules total energy.

A simulation was made of the mode-locked structure (see figure 12) with the same total laser energy in a pulse of constant power level, i.e., square wave. The electron and ion temperature profiles for these two simulations are compared

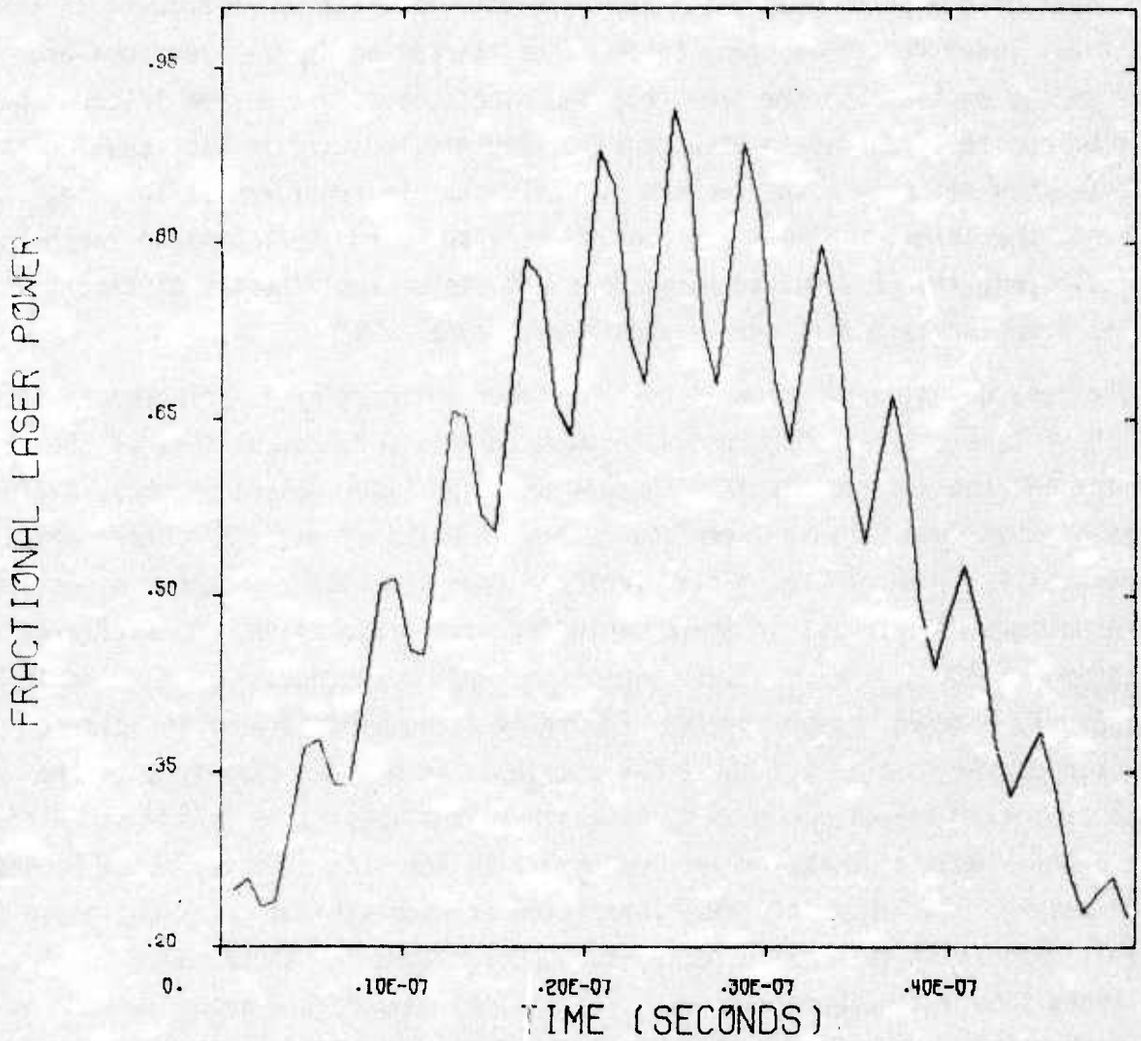

Figure 12. Simulation of Mode Locked CO^2 Laser Pulse, 50 Nanoseconds in Length

in figure 13. Several observations can be made from this comparison: (1) the maximum electron temperature reached in each case is only slightly different and is thus more a function of energy and power than pulse shape; (2) the maximum ion temperature reached in each case is similar, differences are due to ion shock heating; (3) the maximum ion and electron temperatures occur earlier in time than the cutoff of the pulse due to the hydrodynamic expansion which results in lower densities, lower densities cause lower laser absorption in the electrons and lower energy exchange to the ions from the electrons; (4) the time integral of the electron temperatures in each case is very similar; (5) in each case the ions begin cooling off before the electrons, while the electrons are still being heated by the laser, the ions are cooling because of the hydrodynamic expansion. In conclusion, the mode-locked pulse does not yield significantly different results from the "somewhat ideal" square-wave-type pulse.

The next question to arise is how the laser interaction is affected by the scaling of laser power. Figures 14 through 16 show some comparisons of the plasma dynamics and the ion and electron temperatures for laser powers of three different orders of magnitude. These laser powers are in units of ergs/cm/rad/sec which is an azimuthally symmetric laser flux incident upon a cylinder in the $\bar{r}$ direction. For the plasma of interest in these exploding wire calculations, these fluxes correspond to 300 joules/cm, 3,000 joules/cm, and 30,000 joules/cm for the 10^{16}, 10^{17}, and 10^{18} cases, respectively. Figure 14 is a comparison of the plasma outer radius versus time for these three cases. This shows clearly that the effect of the increased power is to blow the plasma apart on a much smaller time scale. The slopes of these curves represent the velocities of the outer boundary of the plasma. Estimates of these velocities for the various cases are given in table 2. Figure 15 is the ion temperature versus time for these power levels. This shows some interesting effects: (1) the ion temperature peaks earlier in time with higher laser power; (2) the width of the temperature versus time peak narrows considerably in time with higher power; (3) there appears to be some optimum laser power for heating the ions because the maximum ion temperature reached in the 10^{16} and 10^{17} cases are each lower than the 10^{17} case. This will be borne out in later comparisons as well. From figure 16, electron temperature versus time for these power levels, the following conclusions can be drawn: (1) the electron temperature appears to have some direct scaling relationship with the laser power (this will be exploited more in a later comparison); (2) the peak in the electron temperature appears earlier in time with the higher laser power,

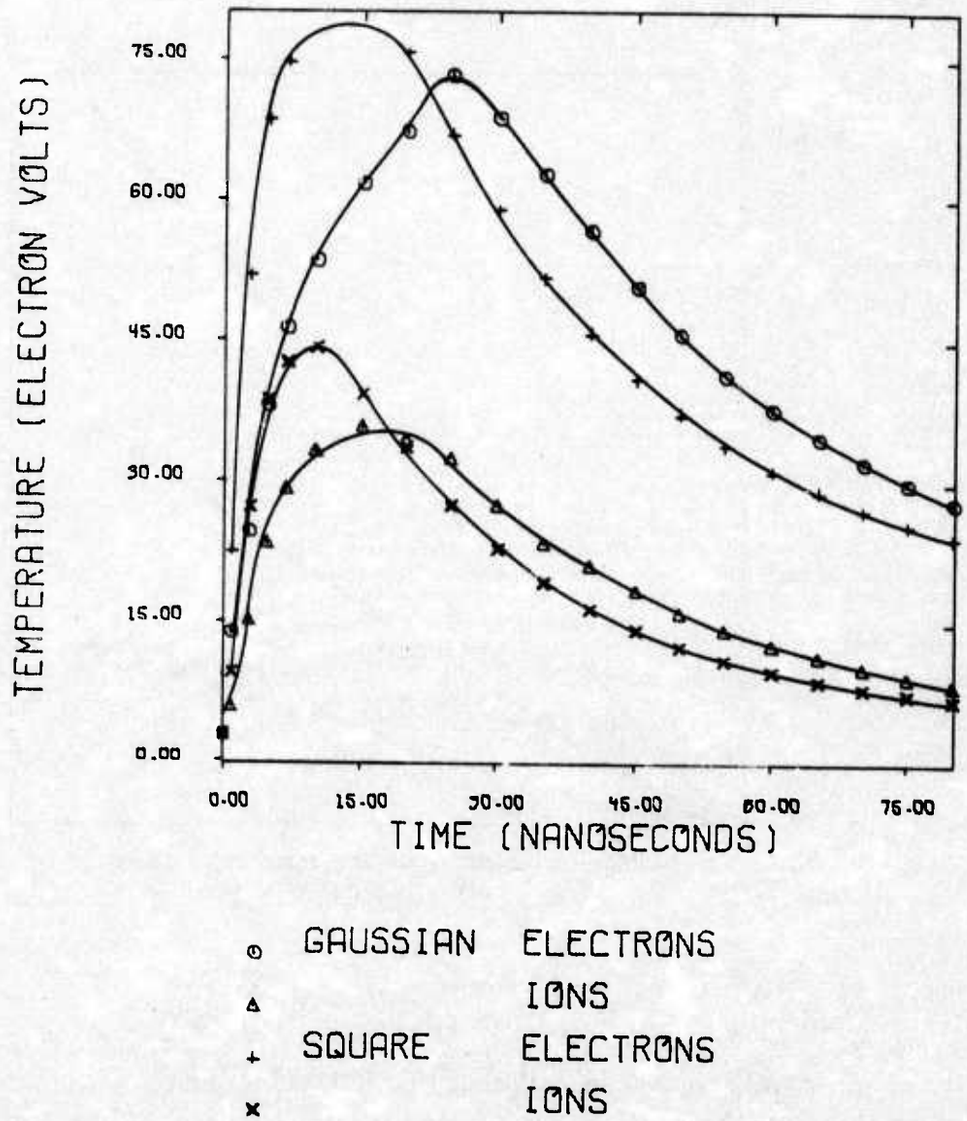

Figure 13. Comparison of Square and Gaussian (Simulated Mode Locked) Pulses of Same Total Energy Incident Upon Initially Identical Plasmas

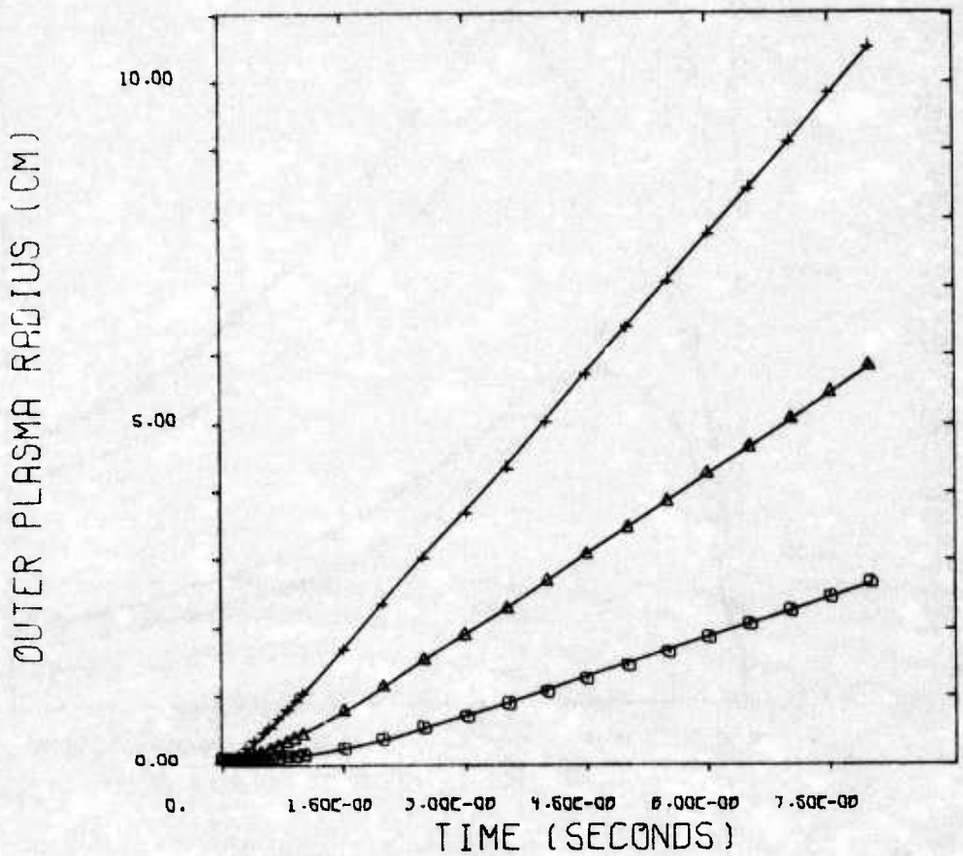

⊙ FLUX=1.0*10**16 ERG/CM/RAD/SEC

△ FLUX=1.0*10**17 ERG/CM/RAD/SEC

+ FLUX=1.0*10**18 ERG/CM/RAD/SEC

Figure 14. Outer Plasma Radius Versus Time as a Function of Laser Power

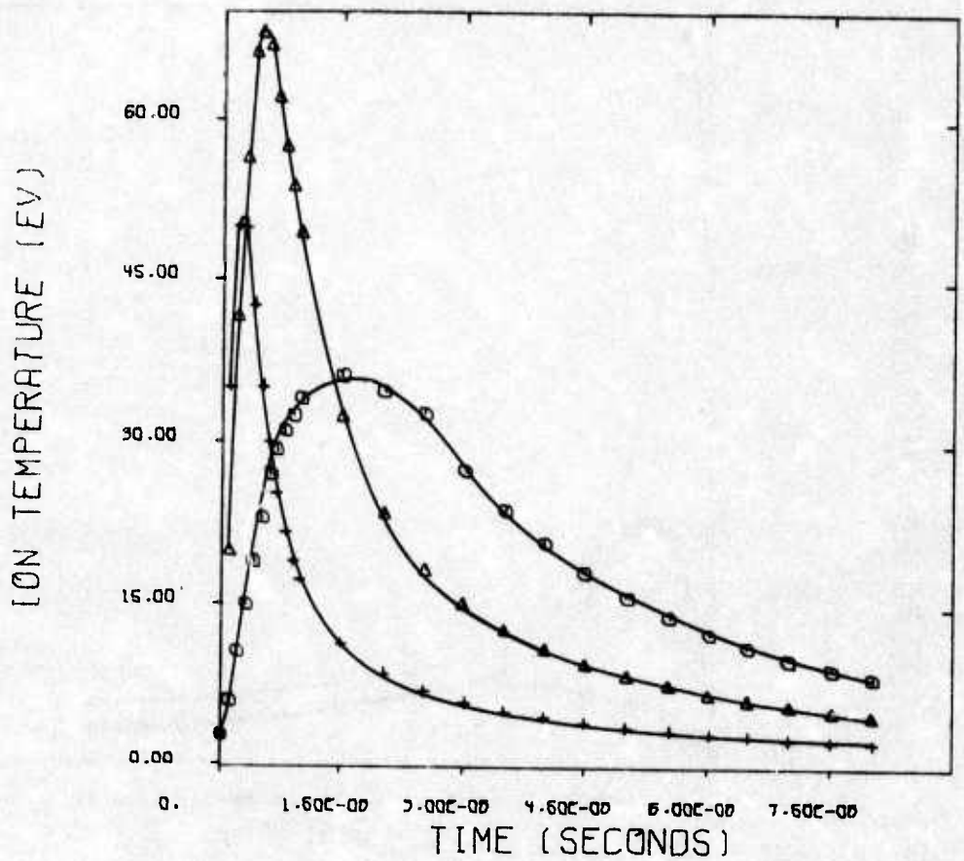

⊙ FLUX=1.0**10**16 ERG/CM/RAD/SEC

△ FLUX=1.0**10**17 ERG/CM/RAD/SEC

+ FLUX=1.0**10**18 ERG/CM/RAD/SEC

Figure 15. Ion Temperature Versus Time as a Function of Laser Power

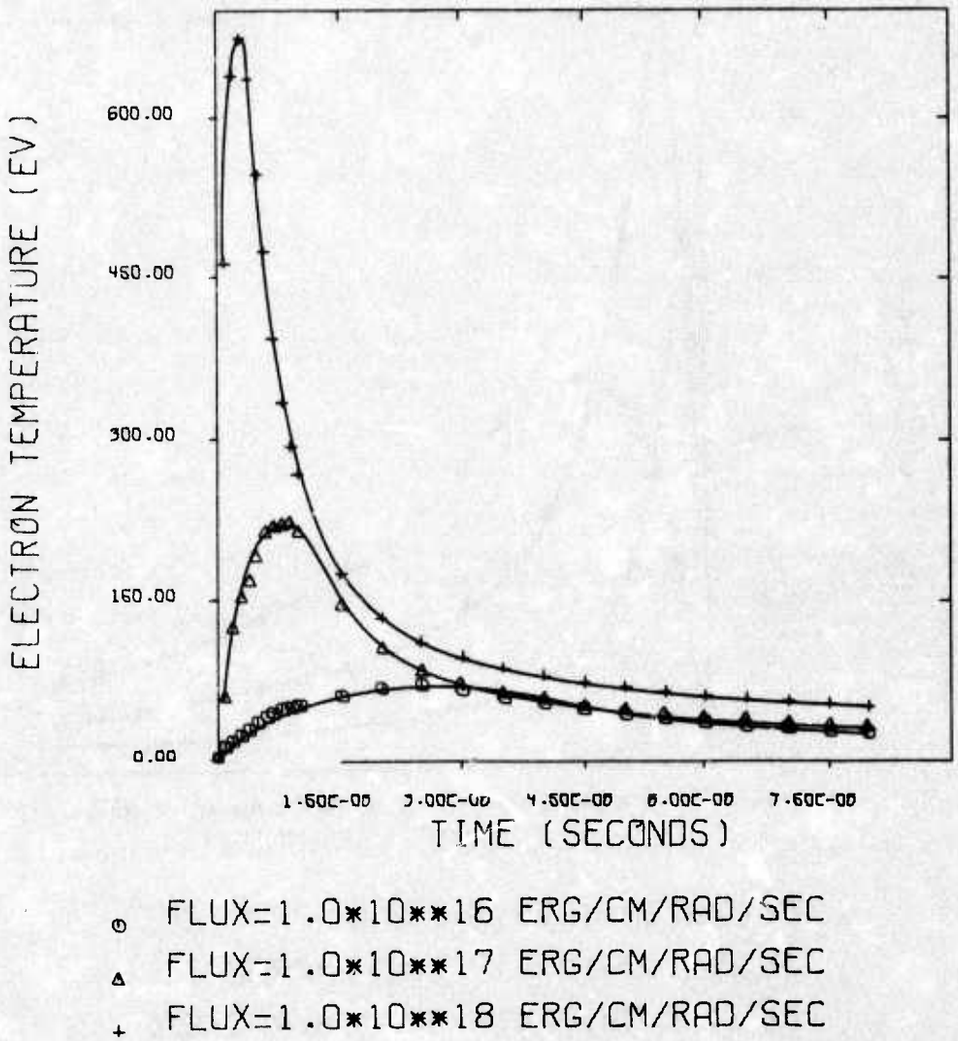

Figure 16. Electron Temperature Versus Time as a Function of Laser Power

Table 2

VELOCITY OF EXPANSION OF OUTER PLASMA BOUNDARY FOR VARIOUS VALUES OF LASER POWER

Laser Power (ergs/cm/rad/sec)	Plasma Velocity (cm/sec)
10^{16}	3.3×10^{7}
10^{17}	7.3×10^{7}
10^{18}	1.3×10^{8}

falling; (3) there appears to be little difference in the late-time (beyond 75 nanoseconds) behavior of the temperature as a function of laser power.

These kinds of comparisons raise a question which is the most pertinent question which can be asked of present simulation experiments; that is, how do these quantities, most importantly ion and electron temperature, scale with laser energy? In other words, are these experiments worth scaling up for simulation purposes? The answering of this question can be helped somewhat with figures 17 and 18. Figure 17 portrays the scaling of maximum electron and ion temperatures versus laser energy for two different laser energy for two different laser pulse lengths. That is, holding the pulse length constant and increasing the energy in the pulse, how does the maximum temperature reached scale with laser energy? Figure 17 uses the laser pulse shape shown in figure 12 with pulse lengths of 10 and 80 nanoseconds. These two pulse lengths are used primarily to give some qualitative comparison of the effect of changing the pulse length. However, numerical relationships in the linear approximation (of a log-log relationship) have been obtained for the scaling in these two cases for the electron temperature alone. The scaling laws are of the following form:

$$T_e^{max} = A\left(E_L\right)^B \tag{35}$$

where T_e^{max} is the maximum electron temperature in electron volts, E_L is the total energy in the laser pulse in joules, and A and B are empirical constants given in table 3. It can be observed, at this point as well, that the relationship of the ion temperature versus laser power hinted at in the discussion of figure 15 can now be clearly demonstrated. There is a laser power or total energy beyond which the maximum ion temperature produced declines with additional incident energy. The hydrodynamic expansion occurs on shorter time scales than

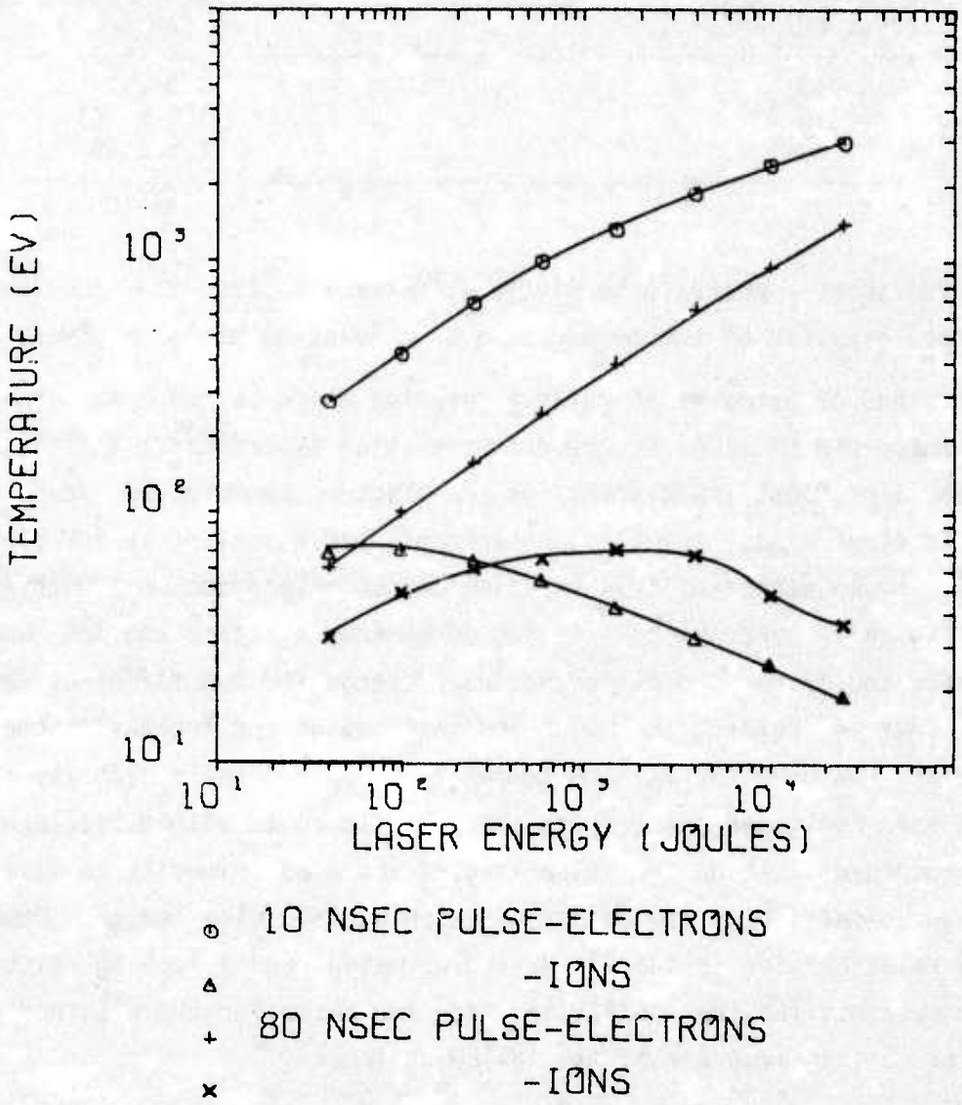

Figure 17. Scaling of Ion and Electron Temperatures (Maximum) as a Function of Incident Laser Energy for Two Pulse Lengths, 10 and 80 Nanoseconds

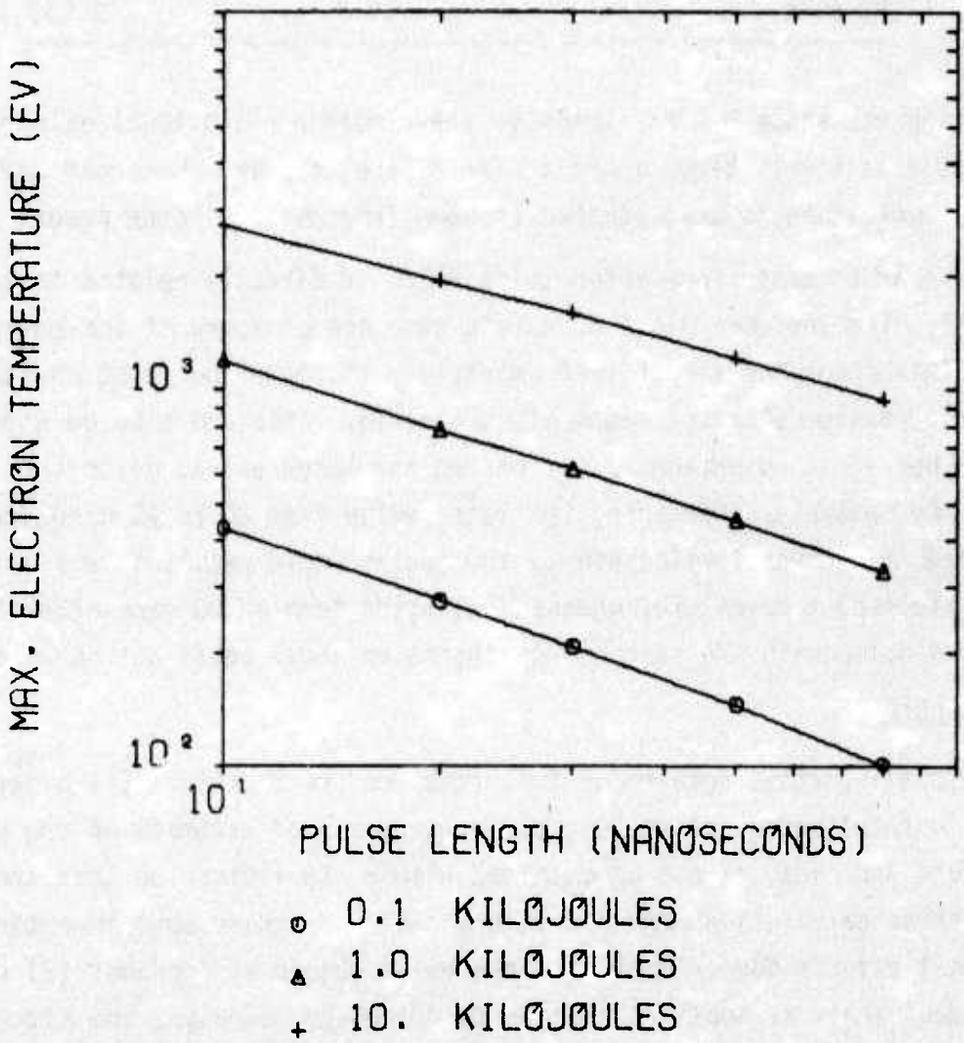

Figure 18. Maximum Electron Temperature Scaling Versus Pulse Length for Total Laser Energy of 0.1, 1.0, and 10 Kilojoules

Table 3

PARAMETERS FOR MAXIMUM ELECTRON TEMPERATURE VERSUS LASER ENERGY FROM EMPIRICAL FITS

Laser Pulse Length	A	B
10 nsec	76.8	0.375
80 nsec	10.3	0.500

the heating via shock hydrodynamics or ion-electron collisional exchange. The plasma is effectively blown apart as far as the ions are concerned and the limiting ion temperature is thus reached at some intermediate laser power.

Figure 18 portrays some information which is directly related to that in figure 17. The contours plotted in this case are contours of iso-energy for the laser. This shows the effect that shortening the laser pulse at constant energy has on the maximum electron temperature reached. This can also be used to determine whether it is advantageous to shorten the laser pulse, given a certain energy change. For example, shortening the laser pulse from 80 to 10 nanoseconds with an energy reduction from 1 kilojoule to 100 joules would result in a slightly higher maximum electron temperature, whereas, changing from an 80-nanosecond to a 30-nanosecond pulse with the same energy change as above would not be advantageous.

3. CONCLUSIONS

The most important results of this research are twofold: (1) given the pulse length and total energy of the CO_2 laser used, a good estimate of the plasma temperature and dynamics can be obtained within the limitation that the codes used in these calculations are one-dimensional and ignore some important two-dimensional effects due primarily to the extra degree of freedom; (2) calculations reveal that, at least in the 40- to 40,000-joule range, the electron temperature reached in the plasma, and thus the radiation output, scale at least weakly with the laser energy at fixed pulse width. The amount of radiation output and the conversion efficiencies are not taken into account in this calculation and are important quantities which remain yet to be determined before any accurate assessment of the simulation possibilities of the exploding wire can be made. It would appear at this juncture that further investigation and research in this area are indeed justified and warranted.

REFERENCES

1. McCann, T. E., Laser Plasma Heating, AFWL-TR-73-61, Air Force Weapons Laboratory, Kirtland AFB, New Mexico, May 1973.

2. McWhirter, R. W. P., "Spectral Intensities," Plasma Diagnostic Techniques (ed. by Huddlestone, R. H. and Leonard, S. L.), Academic Press, New York, 1965.

3. Brueckner, K. A., Hammerling, P., and Thomson, J. A., personal communication, October 1969.

4. Wyatt, R. M., Optical Properties of Laser-Plasma Interactions, AFWL-DYS-TN-73-102, Air Force Weapons Laboratory, Kirtland AFB, New Mexico, December 1973.

5. Shearer, J. W., LRL Document UCID-15745, December 7, 1970.

6. Johnston, T. W. and Dawson, J. M., Phys. Fluids, 16(5), May 1973.

7. Seftor, L., Bull. Amer. Phys. Soc., 18 p. 586, 1973.

8. Stockman, H. S., Jr., Magpie: A User's Manual, AFWL-TR-74-120, Air Force Weapons Laboratory, Kirtland AFB, New Mexico, June 1974.

9. Patterson, S. R., May, T. E., Hunter, R. O., and Kinkade, R. P., "Cold Cathode Electron Beam Sustained CO_2 Laser," Bull. Amer. Phys. Soc., 18, p. 685, 1973.

SYMBOLS

A	atomic weight
C_r'	bremsstrahlung radiation term
E_c	electron thermal conduction term
E_I	ionization energy term
K	inverse bremsstrahlung absorption coefficient
N_e	electron density, cm^{-3}
N_e^c	critical electron density, cm^{-3}
N_i	ion density, cm^{-3}
P_e	electron pressure
P_i	ion pressure
Q_{ei}	ion-electron collisional exchange term
Q_r	bremsstrahlung radiation term
R	zone radius, cm
S_T	thermonuclear reaction rate, sec^{-1}
T_e	electron temperature, °K
Z	atomic number
$\bar{Z}$	average ionization levels
c	speed of light, cm/sec
k	Boltzman constant, ev/°K
kT_e	electron temperature, ev
m_e	electron rest mass
q	electron charge
ε_o	free space permittivity
ε_e	electron internal energy, ergs/gm
ε_i	ion internal energy, ergs/gm

SYMBOL (Cont'd)

$\ell n\Lambda$	classical Coulomb logarithm
ν_L	laser frequency, sec^{-1}
ν_p	plasma frequency, sec^{-1}
τ_0	ion-electron collision time
ϕ	laser flux, ergs/cm/radian/sec
ψ_c	critical optical angle of incidence
$\chi_{g\rightarrow i}(Z)$	ionization potential to remove Zth electron
χ_0'	coefficient of electron thermal conductivity

DISTRIBUTION

No. of Copies	
1	AFA (DFP/Capt T. E. McCann), USAF Academy, CO 80840
1	AFSWC (HO), Kirtland AFB, NM 87117
	AFWL, Kirtland AFB, NM 87117
2	(SUL)
20	(DYS)
2	(DYT)
1	AUL (LDE), Maxwell AFB, AL 36112
2	DDC (TCA), Cameron Sta, Alexandria, VA 22314
1	Official Record Copy to Lt R. M. Wyatt/DYS